Electron spin transport in quantum dots and point contacts

Koop, Erik Johan

Link to publication in University of Groningen/UMCG research database

Chapter 4

Spin accumulation and spin relaxation in a large open quantum dot

Abstract

We report electronic control and measurement of an imbalance between spin-up and spin-down electrons in micron-scale open quantum dots. Spin injection and detection was achieved with quantum point contacts tuned to have spin-selective transport, with four contacts per dot for realizing a non-local spin-valve circuit. This provides an interesting system for studies of spintronic effects since the contacts to reservoirs can be controlled and characterized with high accuracy. We show how this can be used to extract in a single measurement the relaxation time for electron spins inside a ballistic dot ($\tau_{sf} \approx 300$ ps) and the degree of spin polarization of the contacts ($P \approx 0.8$).

This chapter is based on Ref. 5 on p. 131.

4.1   Introduction

The ability to control and detect the average spin orientation of electron ensembles in non-magnetic conductors lies at the heart of spintronic functionalities [1]. We report here electronic control and detection of spin accumulation –an imbalance between the chemical potential of spin-up and spin-down electrons– in a large ballistic quantum dot in a GaAs heterostructure. We use quantum point contacts (QPCs) to operate a four-terminal quantum dot system, which is suited for realizing a non-local spin-valve circuit [2]. Before, such spin-valve circuits were realized with ferromagnetic contacts on various non-magnetic conductors [2, 3, 4], but for these systems it is hard to characterize the contact properties. An interesting aspect of our spintronic system is that it is realized with ultra-clean non-magnetic materials, while each spin-selective mode in the contacts can be controlled individually. We demonstrate that this can be exploited to measure and unravel for a single device the spin relaxation rate inside the dot, contributions to spin relaxation from coupling the dot to reservoirs, and the degree of polarization for spin-selective transport in the contacts. Thus, we report here the spin relaxation time for two different confinement geometries. Chaotic scattering inside such ballistic cavities can result in a spin relaxation mechanism that differs from that of bulk materials and very small few-electron quantum dots [5], but its full understanding is still a challenge to the community [6].

Figure 4.1a presents our device. Depletion gates on a heterostructure with a two-dimensional electron gas (2DEG) below the surface are used to define the four-terminal dot. QPCs are operated as spin-selective contacts, using that the subbands that carry the ballistic transport can be Zeeman split with a strong in-plane magnetic field, and that these modes can be opened up one by one by tuning gate voltages [7, 8]. The conductance of QPCs then increases in steps, with plateaus at Ne^2/h, where N the number of open modes. For odd (even) N the last opened mode carries only spin-up (spin-down). For the most typical form of our experiment we tune to the following setting. The QPC to the $I+$ reservoir has a single open mode, which is only available for spin-up electrons, while the $I-$ QPC is tuned to carry one mode for spin-up and one for spin-down, and we apply here a current I_{bias}. The contact resistance for electrons entering the dot via $I-$ is equal for spin-up and spin-down, while the current that leaves the dot carries only spin-up. Consequently, the chemical potential for spin-down electrons inside the dot will become higher than that for spin-up, up to a level that is limited by spin relaxation. This difference in chemical potential $\Delta\mu_{\uparrow\downarrow}$ can
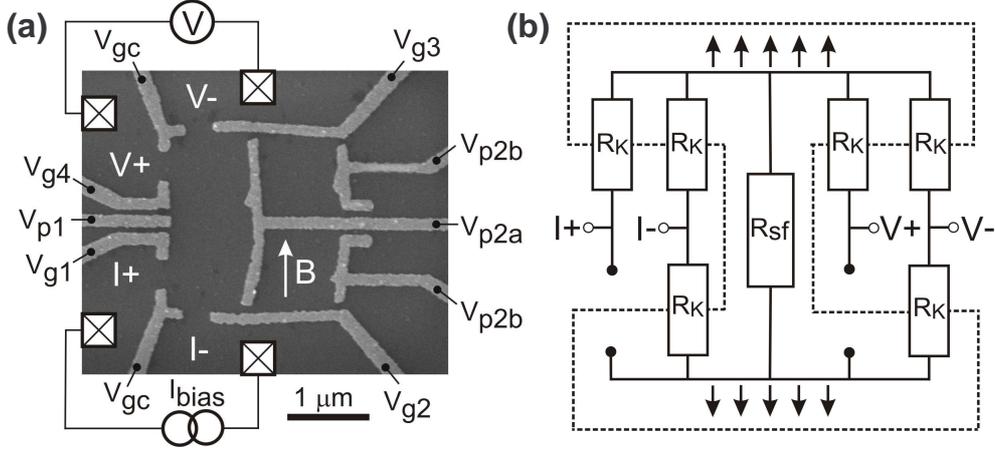
Figure 4.1: (a) Electron microscope image of the device, with labels for current and voltage contacts, and depletion gates V_{gi} and V_{pi}. Gate V_{p1} is a shape distorting gate. Fully switching gate V_{p2a} or gates V_{p2b} on or off sets the overall size of the dot, but fine tuning these gates is also used for controlling small shape distortions. **(b)** Resistor model for the most typical experiment (see text), for the case of ideal spin polarization of the contacts to the $I+$ and $V+$ reservoirs. The spin-up (top) and spin-down (bottom) populations inside the dot are contained within the dashed line. The spin-flip resistance R_{sf} represents spin relaxation inside the dot.

be measured as a voltage: with the $V+$ QPC tuned to have only one open mode for spin-up and the $V-$ QPC tuned to have one open mode for spin-up and one for spin-down, the voltage is $V = \Delta\mu_{\uparrow\downarrow}/2e$, which is for linear response expressed as a non-local resistance $R_{nl} = V/I_{bias}$.

4.2 Resistor Model

The resistor model in Fig. 4.1b is useful for analyzing how spin-relaxation mechanisms influence the measured signal in the above experiment. Each open mode for spin-up in a QPC is modeled as a resistor with value $R_K = h/e^2$ to the spin-up population in the dot, and similar for spin-down (we assume first perfect polarization of QPCs tuned to be spin selective). Spin-relaxation *inside* the dot is modeled as a resistor R_{sf} that carries a current from the spin-up to the spin-down population. Figure 1b illustrates that the contacts to the $I-$ and the $V-$ reservoir provide additional current paths for relaxation parallel to R_{sf} (spins rapidly mix in reservoirs, and reservoirs always have zero spin-accumulation). This mechanism for spin relaxation *outside* the dot causes that in the limit of

$R_{sf} \rightarrow \infty$ (no relaxation inside the dot), R_{nl} is limited to $R_K/4$. The voltage that is driving the relaxation inside the dot is $\Delta\mu_{\uparrow\downarrow}/e$, while the current through R_{sf} is $I_{sf} = e\Delta\mu_{\uparrow\downarrow}/2\Delta_m\tau_{sf}$, such that the spin-flip time τ_{sf} dictates R_{sf} according to $R_{sf} = 2\tau_{sf}\Delta_m/e^2$ [9]. Here $\Delta_m = 2\pi\hbar^2/m^*A$ is the mean energy spacing between spin-degenerate levels in a dot of area A. Consequently, measuring R_{nl} and deriving R_{sf} from its value can be used for determining τ_{sf}. While this resistor model does not account for various mesoscopic effects that occur in ballistic chaotic quantum dot systems, a theoretical study of an equivalent two-terminal spintronic dot [6] showed that it is valid in the regime that applies to our experiment (no influence of weak-localization and Coulomb blockade effects), and we indeed find that it is consistent with the measured spin signals that we report.

4.3   Experimental realization

The dot was realized in a $GaAs/Al_{0.32}Ga_{0.68}As$ heterostructure with the 2DEG at 114 nm depth. At 4.2 K, the mobility was $\mu = 159$ m^2/Vs and the electron density $n_s = (1.5 \pm 0.1) \cdot 10^{15}$ m^{-2}. For gates we used electron-beam lithography and lift-off techniques, and deposition of 15 nm of Au on a Ti sticking layer. The reservoirs were connected to wiring via Ohmic contacts, which were realized by annealing Au/Ge/Ni from the surface. All measurements were performed in a dilution refrigerator at an effective electron temperature $T_{eff} \approx 100$ mK. For measuring R_{nl} we used lock-in techniques at 11 Hz with a current bias, where we made sure that the associated bias voltage $V_{bias} \leq 10$ μV. We carefully checked that RC-effects did not influence R_{nl} results. We used the T-shaped gate V_{p2a} or pair of gates V_{p2b} for setting the *overall size* of the dot (not to be confused with tuning small shape distortions for averaging out fluctuations, see below) at either an area of 1.2 μm^2 or 2.9 μm^2 (accounting for a depletion width of $\sim$ 150 nm around the gates).

4.4   Results of non-local experiments

Before presenting measurements of spin accumulation, we discuss two effects that make this experiment in practice less straight forward than in the above description. Quantum fluctuations in R_{nl} due to electron interference inside the dot [10] have an amplitude that is comparable to the spin signal [11], and R_{nl} can only be studied as a spin signal after averaging over a large number of fluctuations. The inset of Fig. 4.2b shows such fluctuations in R_{nl} as a function of the voltage on
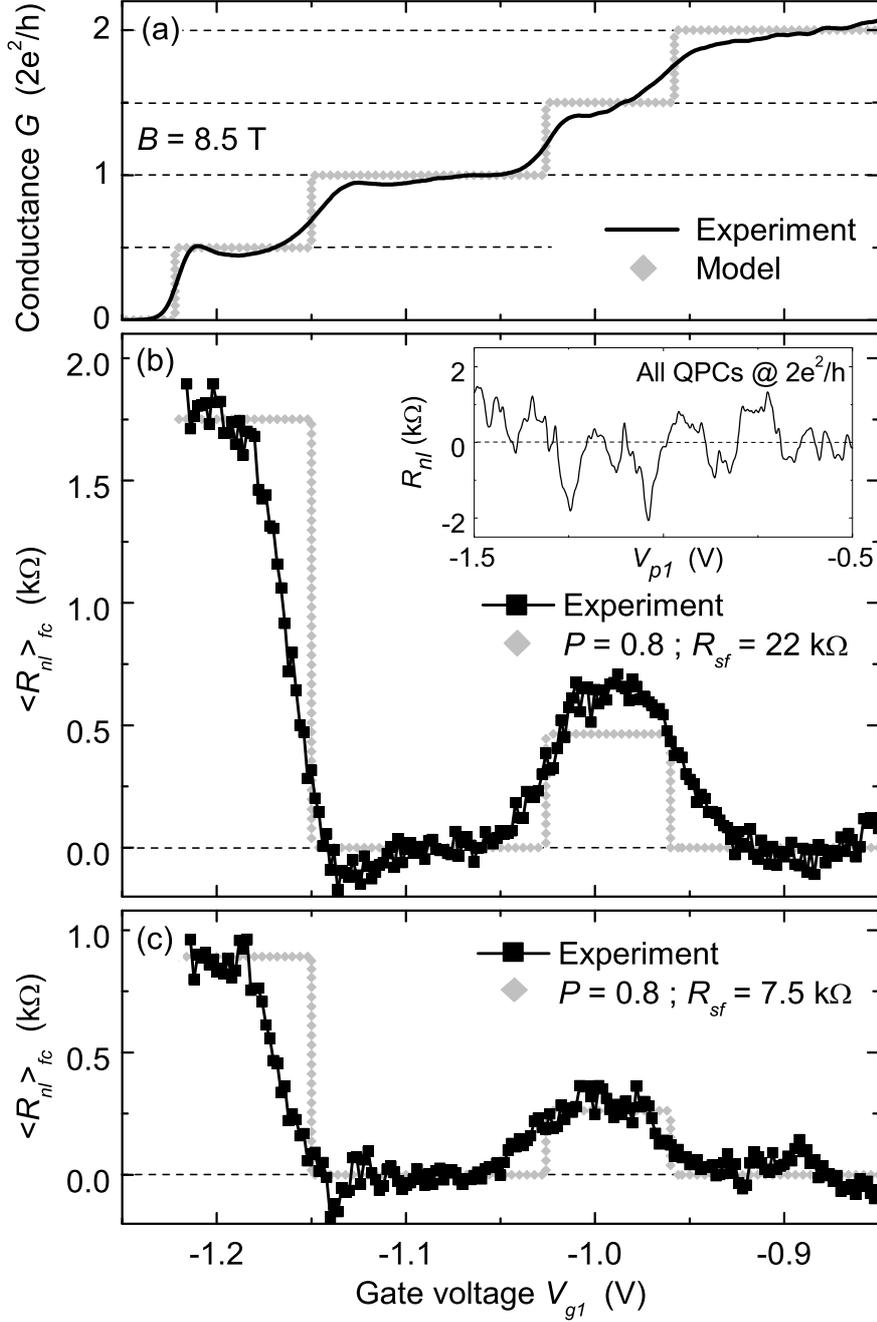
Figure 4.2: **(a)** Conductance G of the QPC to the $I+$ reservoir as a function of gate voltage V_{g1}, measured at $B = +8.5$ T. Gray diamonds indicate the values for conductance that we use in the resistor model, where we assume sharp transitions between conductance plateaus. **(b)**,**(c)** Non-local resistance results $\langle R_{nl}\rangle_{fc}$ as a function of gate voltage V_{g1} (controlling the number of open modes in the $I+$ QPC) for the dot with area 1.2 μm^2 **(b)** , and 2.9 μm^2 **(c)**. Gray lines show R_{nl} values from the resistor model, with the spin-flip resistance R_{sf} and polarization P as in the figure labels. The inset in **(b)** shows fluctuations of R_{nl} as a function of shape gate V_{p1} with all QPCs at a conductance of $2e^2/h$.

V_{p1}, which causes a small shape distortion of the dot. We discuss results as $\langle R_{nl} \rangle$ when presenting the average of 200 independent R_{nl} fluctuations, from sweeping with two different shape-distorting gates. Cross talk effects between gates were carefully mapped out and compensated for keeping the QPCs at their desired set points [12].

A second effect which, besides spin accumulation, may result in strong R_{nl} values is electron focusing [11]. Our sample was mounted with its plane at $0.73°$ with respect to the direction of the total magnetic field B. Consequently, there is a small perpendicular field $B_\perp$ and the associated electron cyclotron diameter equals the $I+$ to $V+$ contact distance (Fig. 4.1a) at $B = \pm 6$ T. We will mainly present results measured at $B = +8.5$ T, for which we found that focusing only weakly influences $\langle R_{nl} \rangle$ results. Further, we use that we can subtract a background contribution to $\langle R_{nl} \rangle$ from focusing (discussed below), and we present results where this is applied as $\langle R_{nl} \rangle_{fc}$. $B_\perp$ also breaks time-reversal symmetry (suppressing weak localization) when $|B| > 0.2$ T.

Figure 4.2b presents $\langle R_{nl} \rangle_{fc}$ as a function of the number of open modes in the $I+$ contact (tuned by V_{g1}), while the other QPCs are tuned as in Fig. 4.1b. On the left on this V_{g1} axis, the $I+$ QPC carries only one spin-up mode (conductance G_{I+} tuned to the e^2/h plateau, see also Fig. 4.2a). Here $\langle R_{nl} \rangle_{fc} \approx 1.8$ kΩ. Tuning V_{g1} to more positive values first adds an open spin-down mode to the $I+$ QPC (G_{I+} at $2e^2/h$), such that it is no longer spin selective and $\langle R_{nl} \rangle_{fc}$ drops here indeed to values near zero. Further opening of the $I+$ QPC tunes it to have two spin-up modes in parallel with one-spin down mode ($G_{I+} = 3e^2/h$). This causes again a situation with more spin-up than spin-down current in the $I+$ QPC, but less distinct than before and here $\langle R_{nl} \rangle_{fc}$ shows again a clear positive signal. Then, it drops to zero once more when the next spin-down mode is opened in the QPC. We obtain nominally the same results when the role of the current and voltage contacts is exchanged. Further, Fig. 4.2c shows that the large dot shows the same behavior, but with lower $\langle R_{nl} \rangle_{fc}$ values. This agrees with a lower value for R_{sf} for the large dot. From these measurement we can conclude that $\langle R_{nl} \rangle_{fc}$ is a signal that is proportional to the spin accumulation $\Delta \mu_{\uparrow \downarrow}$ in the dot.

The conductance of the $I+$ QPC, shown in Fig. 4.2a, displays multiple clear conductance plateaus that appear at the expected conductance values, although there are several bumps and dips in these plateaus. Especially at the e^2/h conductance plateau there is a pronounced resonance. However, a similar feature, a small peak followed by a dip for going to more positive gate voltages, can be seen at the $2e^2/h$ plateau. In zero magnetic field also similar features appear for the
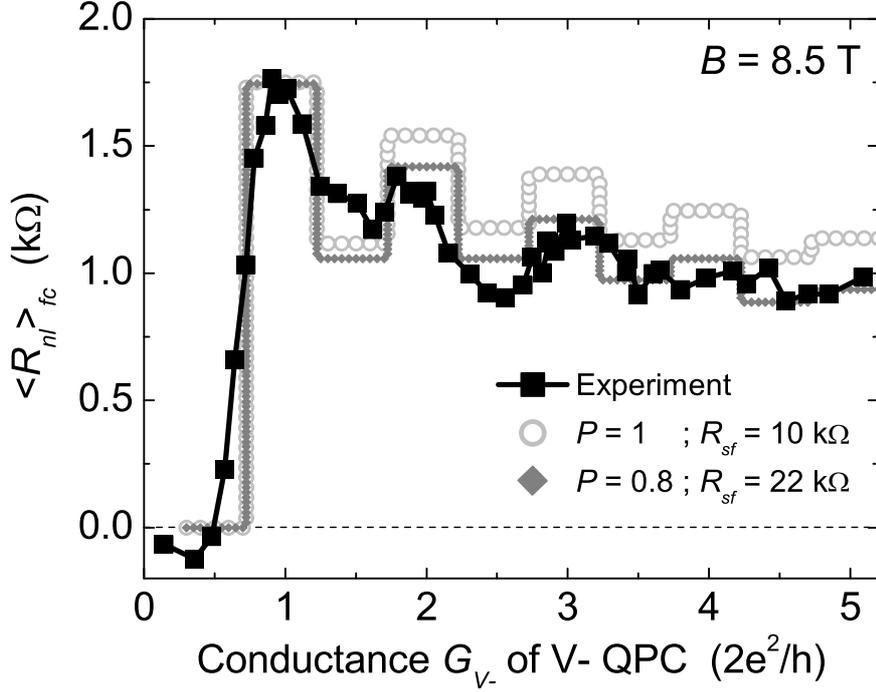
Figure 4.3: Averaged non-local resistance $\langle R_{nl} \rangle_{fc}$ as a function of the conductance G_{V-} of the V- QPC, for $A = 1.2$ μm^2. Gray lines show R_{nl} values from the resistor model, with the spin-flip resistance R_{sf} and polarization P as labeled.

first three conductance plateaus (not shown). Because the conductance plateaus do appear around the expected values, and the resonant feature appears in the same way for different plateaus, we think that the opening-up of subbands is not influenced significantly and our analysis as presented above is correct.

Figure 4.3 shows results from a similar experiment on the small dot (but also here the large dot showed the same behavior). Now $\langle R_{nl} \rangle_{fc}$ is measured as a function of the number of open modes in the $V-$ QPC (tuned by V_{g3}), while all other QPCs are again tuned as in Fig. 4.1b. Here we observe a signal close to zero when the $V-$ QPC carries only one spin-up mode ($G_{V-} = e^2/h$) since it then probes the same chemical potential as the $V+$ QPC. Opening it to $G_{V-} = 2e^2/h$ immediately results in a strong signal. Further opening this QPC then causes the signal to go up and down, qualitatively in reasonable agreement with the resistor model that assumes perfect polarization ($P = 1$) of each spin-selective mode in a QPC (see theory traces in Fig. 4.3, these go up and down in a step-like manner since we assume sharp transitions between conductance plateaus). However, with quantitative agreement at $G_{V-} = 2e^2/h$ (for $R_{sf} = 10$ kΩ), this

model with $P = 1$ shows an average slope down with increasing G_{V-} that is too weak. Instead, we find that the resistor model can show quantitative agreement over the full G_{V-} range (and with the results in Fig. 4.2) when we account for imperfect spin polarization of QPCs.

We model imperfect polarization in the resistor model as follows. We assume it only plays a role for QPCs set to a conductance of Ne^2/h, with N an odd integer (because the energy spacing between pairs of Zeeman-split subbands is large [8]). Spin-selective transport is then only due to the highest pair of subbands that contributes to transport, and *we define the polarization P only with respect to this pair*. This pair of subbands is then modeled as a resistor $R_\uparrow = 2R_K/(1 + P)$ to the spin-up population in the dot, and a resistor $R_\downarrow = 2R_K/(1 - P)$ to the spin-down population, which corresponds to $P = (R_\downarrow - R_\uparrow)/(R_\downarrow + R_\uparrow)$. This provides a simple model for R_{nl} with only R_{sf} and P as fitting parameters if we assume that all spin-selective QPCs and QPC settings can be modeled with a single P value. We find then a good fit to all the data in Figs. 4.2 and 4.3 for $P = 0.8 \pm 0.1$, with $R_{sf} = 22 \pm 3$ kΩ for the small dot and $R_{sf} = 7.5 \pm 1$ kΩ for the large dot. In Fig. 4.2b at $G_{I+} = 3e^2/h$, the experimental results are higher than the plotted model values. However, this turns into the opposite situation when using results obtained with the current and voltage QPCs exchanged. This indicates that P does not have exactly the same value for all QPCs and QPC settings. There is, however, always agreement with the model when accounting for the error bars of P and R_{sf}.

The values of R_{sf} correspond to $\tau_{sf} = 295 \pm 40$ ps for the small dot and $\tau_{sf} = 245 \pm 35$ ps for the large dot. In our type of system spin relaxation in the dot is probably dominated by Rashba and Dresselhaus spin-orbit coupling. How this mechanism results in a certain value for τ_{sf} then depends on the ballistic scattering rate at the edge of the dot. We performed numerical simulations of this mechanism, which yield that relaxation times indeed depend on the size of the dot, with typical values near 300 ps [5]. In our experiment, however, the error bars for τ_{sf} are too large for studying this dependence on the shape of our dots, but our method is suited exploring this topic in future work.

Figure 4.4 shows how focusing affects $\langle R_{nl} \rangle$ and $\langle R_{nl} \rangle_{fc}$. For QPCs tuned as in Fig. 4.1b the signal from spin accumulation drops to zero if either the $I+$ or the $V+$ QPC is tuned from e^2/h to $2e^2/h$ (no longer spin selective). However, when sweeping B we also measure large positive and negative $\langle R_{nl} \rangle$ values when the $I+$ QPC, the $V+$ QPC or both are at $2e^2/h$. For these three settings we observed $\langle R_{nl} \rangle$ traces that are nominally the same (black symbols in Fig. 4.4a).
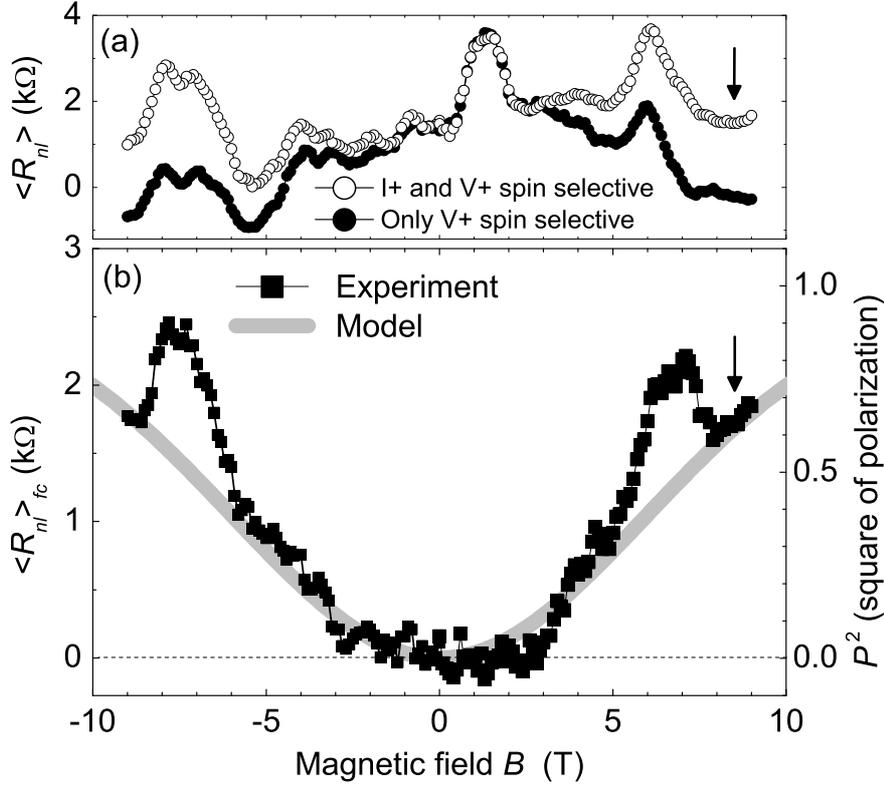
Figure 4.4: **(a)** Averaged non-local resistance $\langle R_{nl} \rangle$ as a function of B, for $I+$ and $V+$ at the e^2/h spin-polarized conductance plateau (open symbols), and for $I+$ at $2e^2/h$ (not spin selective) and only $V+$ at e^2/h (closed symbols). The $I-$ and $V-$ QPCs are at $2e^2/h$, $A = 1.2$ μm^2. The difference in $\langle R_{nl} \rangle$ for the traces in (a) defines the focussing corrected non-local resistance $\langle R_{nl} \rangle_{fc}$, shown in **(b)**. The gray line in **(b)** is a fit of the model where the polarization P of QPCs (right axis) increases with Zeeman-splitting (see text). Arrows indicate B that was applied for measuring the data of Figs. 4.2, 4.3.

The peaked structure is due to electron focusing effects [7, 11]. Only the peak at $+6$ T corresponds to direct focusing from the $I+$ into the $V+$ contact without an intermediate scatter event on the edge of the dot (it has the right B value and other peaks move to other B values when comparing the small and the large dot). Note, however, that all $\langle R_{nl} \rangle$ values are significantly higher when both the $I+$ and $V+$ QPC are tuned to be spin selective (open symbols in Fig. 4.4a). This difference between the open and black symbols defines the quantity $\langle R_{nl} \rangle_{fc}$ (Fig. 4.4b) and provides a signal that is mainly due to spin. This $\langle R_{nl} \rangle_{fc}$ data also shows a peaked structure where $\langle R_{nl} \rangle$ shows strong focusing signals. This agrees

with enhancement of electron focusing signals between spin-selective QPCs [7].

For interpreting $\langle R_{nl} \rangle_{fc}$ as a measure for spin accumulation, the experiment must be performed in a regime with many chaotic scatter events inside the dot during the electron dwell time. This is clearly not the case at the focusing peaks in Fig. 4.4b (at -7.5 T and $+6$ T). We therefore studied spin accumulation at $+8.5$ T where focusing from the $I+$ QPC scatters on the edge of the dot just before the $V+$ contact and where the signatures of focusing in $\langle R_{nl} \rangle$ are small. The agreement between the results of both Figs. 4.2 and 4.3, for both the small and large dot, and the resistor model supports the conclusion that these results were obtained in a chaotic regime.

As a final point we discuss that the degree of polarization $P = 0.8$ is in agreement with independently determined QPC properties. Steps between conductance plateaus are broadened by thermal smearing (a very weak contribution for our QPCs at 100 mK) and due to tunneling and reflection when the Fermi level E_F is close to the top of the QPC potential barrier for the mode that is opening. It is mainly this latter effect that causes $P < 1$ in our experiments. The role of tunneling and reflection in QPC transport is described with an energy dependent transmission $T(\epsilon)$ that steps from 0 to 1 when a QPC mode is opened. We study the effect of this on P by assuming that E_F is located exactly between the bottoms of a pair of Zeeman split subbands. For these two subbands we use $T(\epsilon)_{\uparrow(\downarrow)} = (\mathrm{erf}(\alpha(\epsilon - E_F - (+)E_Z/2)) + 1)/2$, a phenomenological description that agrees with studies of our QPCs [8]. Here $E_Z = g\mu_B B$ is the Zeeman splitting (for g-factor g and Bohr magneton μ_B) and α a parameter that sets the width of the step in $T(\epsilon)$. For $eV_{bias} < k_B T_{eff}$, the contributions of these two subbands to the QPC conductance are then $G_{\uparrow(\downarrow)} = (e^2/h) \int d\epsilon \, (-df/d\epsilon) \, T(\epsilon)_{\uparrow(\downarrow)}$, where f the Fermi function. With $P = (G_\uparrow - G_\downarrow)/(G_\uparrow + G_\downarrow)$ we now calculate how P increases with B due to an increasing Zeeman splitting. In the resistor model the dependence of R_{nl} on P is close to $R_{nl} \propto P^2$. We therefore plot P^2 in Fig. 4.4b (gray line, with scaling of the right axis such that it overlaps with the experimental results) for parameters that give the consistent result $P = 0.8$ at $B = 8.5$ T. For this we use $|g| = 0.44$ (as for bulk GaAs) and an α value that is derived from a full-width-half-max of 0.2 meV for the peak in $dT(\epsilon)/d\epsilon$. The latter parameter agrees with the values 0.20 to 0.35 meV that we found when characterizing this for our QPCs [8]. Notably, we cannot calculate such a consistent result if we assume that the many-body effects that we observed in our QPCs [8] enhance the Zeeman splitting (showing for example $|g| \approx 1.1$). This indicates that these effects do not play a role for spin injection and detection with QPCs, as was also

found in Ref. [7].

4.5   Signatures of spin transport in the 2-terminal conductance

We investigate signatures of spin accumulation and spin relaxation in the two-terminal conductance of our QD, as an alternative to the non-local measurement geometry [6, 13]. This method should, in principle, make the experiment less complex since only two QPCs have to be set simultaneously, instead of four in the non-local experiment. In practice this method is complicated by the additional requirement that one needs broad, flat (spin-selective) conductance plateaus to reliably determine the signatures of spin accumulation in the series conductance of the dot [6, 13].

The system is tuned to the following setting. The QPC to the $I+$ reservoir is tuned to have a single open mode, which is only available for spin-up electrons, while the QPC to the $I-$ reservoir is tuned to carry one mode for spin-up and one mode for spin-down. Initially all other QPCs are pinched-off. With these settings the series conductance of the QPCs is $\frac{1}{4}(2e^2/h)$ if there is no spin relaxation and $\frac{1}{3}(2e^2/h)$ if there is strong spin relaxation. The measured value of conductance will typically lie in between these two limits and can be used to extract the spin relaxation time [13]. Further we can measure the 2-terminal series conductance while we open a third QPC to a large (floating) electron reservoir. This provides an additional relaxation mechanism for loss of spin accumulation, and will allow us to not only extract a value for the spin flip time, but also to identify contributions to spin relaxation from coupling the dot to reservoirs, and the degree of polarization for spin-selective transport in the contacts.

Here we will present some preliminary data on this type of experiment. We have corrected for quantum fluctuations in G due to electron interference inside the dot by averaging over 200 independent fluctuations. The measurements were done at $B = 9$ T, but we have not studied the effects of focussing carefully.

Fig. 4.5a presents $\langle G \rangle$ as a function of the number of open modes in the $I+$ contact (tuned by V_{g1}). The $I-$ contact was tuned to have one spin-up and one spin-down mode. When the $I+$ QPC is tuned to a spin degenerate plateau we measure the same two-terminal conductance for each of the three different dot areas. We do expect to measure a difference in conductance when the $I+$ QPC is at a spin selective plateau. Indeed, when the $I+$ QPC is tuned to the e^2/h
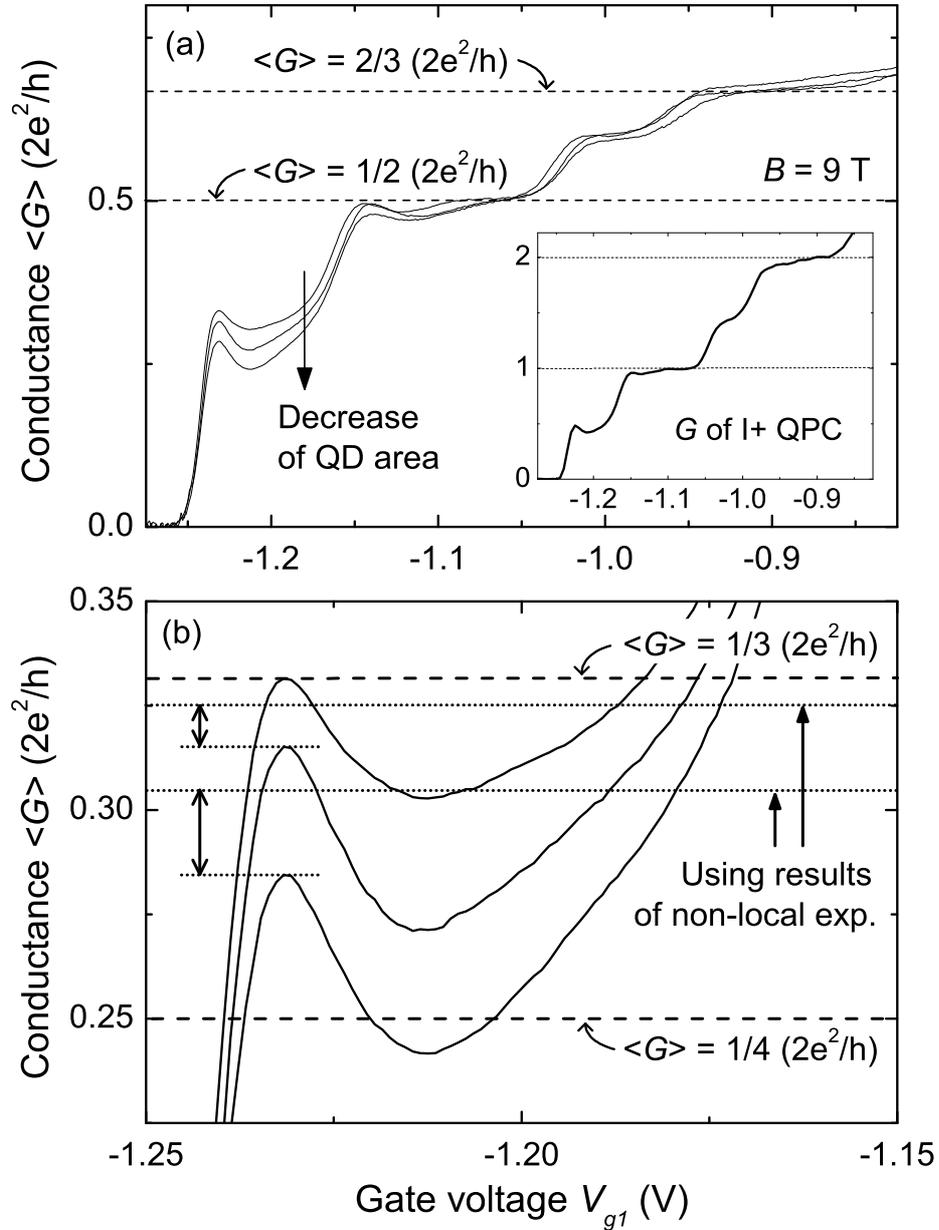
Figure 4.5: **(a)** Average two-terminal conductance $\langle G \rangle$ as a function of gate voltage V_{g1} (controlling the number of open modes in the $I+$ QPC), for the dot with area 1.2 μm^2, 2.9 μm^2, and 10000 μm^2 measured at $B = 9$ T. The $I-$ QPC is set to $2e^2/h$. The dashed lines indicate conductance values where both QPCs are set to spin degenerate plateaus. **(b)** Enlarged view of the data in **(a)** at the gate voltage range where the conductance of the $I+$ QPC is around e^2/h. Dashed lines indicate the two limits for spin relaxation. Dotted lines and arrows on the left indicate the difference between current experiment and expected values using results of the non-local experiment.

plateau we observe a clear difference between the three traces, we find a smaller value for the conductance for a decrease in dot area. When the $I+$ QPC is tuned to $3e^2/h$ we do not observe any significant difference.

We now focus on the situation where the $I+$ is tuned to e^2/h. We then expect to measure plateau heights that are in between the two limits of $\frac{1}{4}(2e^2/h)$ and $\frac{1}{3}(2e^2/h)$. However, as shown in Fig. 4.5a, the conductance plateau is far from a broad, flat plateau. This is a result of the resonance in the e^2/h plateau of the $I+$ QPC shown in the inset of Fig. 4.5a (and in Fig. 4.2a for $B = 8.5$ T). The question is therefore what value of the conductance we should use as plateau height. We choose to use the value of the conductance at the small peak near V_{g1} = -1.23 V, for two reasons. Firstly, in the measured conductance of the QPC to the $I+$ reservoir, the conductance value at the peak is exactly equal to $0.5(2e^2/h)$. Secondly, at the peak in the series conductance for the largest dot with area $\sim$ 10000 μm^2, the value of the conductance is, as expected, equal to $\frac{1}{3}(2e^2/h)$, the limit where all spins can relax. The reason why we did not choose any other combination of QPCs for this experiment is that none of the other QPCs had a broad, flat e^2/h plateau, or, in other words, a plateau that would allow easier determining of the exact value of the conductance at the plateau.

Earlier in this chapter we have measured the relaxation time for the two smallest dots and, using the resistor model, we can use these times to calculate the two-terminal conductance that we expect to measure. Here we have used $\tau_{sf} = 295$ ps for a dot of 1.2 μm^2 and $\tau_{sf} = 245$ ps for a dot of 2.9 μm^2. We also used polarization $P = 0.8$ for the contacts. If we compare these calculated values to the values we measure here, we find that we observe here in both cases a lower value for conductance (also if we include error bars of τ_{sf} and P). This could mean we measure much longer relaxation times in this experiment, however we believe that these measured conductances are not reflecting properties of the spin accumulation in the dot, but are determined by the same phenomenon that causes the resonant-like feature to appear. Therefore we decided not to continue with this type of experiment on this particular device.

4.6   Conclusions

In conclusion, we have observed spin accumulation in a large open quantum dot in a non-local measurement and extracted values for τ_{sf} and P. We find values of $\tau_{sf} = 295 \pm 40$ ps for a dot of 1.2 μm^2 and $\tau_{sf} = 245 \pm 35$ ps for a dot of 2.9 μm^2. These values are much lower than reported values from studies on

large high-mobility 2DEG areas. This is probably due to enhanced dephasing by spin-orbit effects which results from frequent scattering on the edge of the dot. We can reproduce this effect qualitatively with Monte-Carlo simulations, presented in Chapter 5 of this thesis. The values of $P = 0.8 \pm 0.1$ that we find, are consistent with the short length ($\sim$100 nm) of our QPCs. The short length causes a broad energy window where the onset of the transmission of each QPC mode builds up, such that two Zeeman split modes still overlap considerably in a field of 9 T. Notably, our data set is consistent with a Zeeman energy that is simply $g\mu_B B$ with $g = 0.44$, indicating that many-body effects in QPC that can enhance Zeeman splittings do not play a role in our type of experiment. We have been made aware of related results obtained by S. M. Frolov *et al.* [14] with a narrow Hall bar.

We have presented a method for extracting spin relaxation times from the two-terminal conductance of a quantum dot, inspired by experimental results of Zumbühl *et al.* [13] and theory paper by Beenakker [6]. We have studied this two-terminal conductance for dots with three different areas, but unfortunately the spin-resolved plateau at e^2/h for one of the contacts was disturbed by a pronounced resonance. Therefore we could not extract reliable numbers for spin relaxation time or polarization using this method.

References

[1] For a recent review see D. D. Awschalom and M. E. Flatté, Nat. Phys. **3**, 153 (2007).

[2] F. J. Jedema *et al.*, Nature **410**, 345 (2001).

[3] X. Lou *et al.*, Nat. Phys. **3**, 197 (2007).

[4] N. Tombros *et al.*, Nature **448**, 571 (2007).

[5] E. J. Koop *et al.*, arXiv:0804.2968.

[6] C. W. J. Beenakker, Phys. Rev. B **73**, 201304(R) (2006).

[7] R. M. Potok *et al.*, Phys. Rev. Lett. **89**, 266602 (2002).

[8] E. J. Koop *et al.*, J. Supercond. Nov. Magn. **20**, 433 (2007).

[9] M. Johnson, Phys. Rev. Lett. **70**, 2142 (1993).

[10] Y. Alhassid, Rev. Mod. Phys. **72**, 895 (2000).

[11] A. I. Lerescu *et al.*, arXiv:0705.3179.

[12] D. R. Stewart, PhD thesis, Stanford University (1999).

[13] D. M. Zumbühl *et al.*, 2001 March Meeting Bulletin of the American Physical Society (unpublished), Abstract C25.006 (2001).

[14] S. M. Frolov *et al.* arXiv:0801.4021 (2008).